Nanoscale Advances

ROYAL SOCIETY OF CHEMISTRY

PAPER

View Article Online
View Journal | View Issue

Cite this: *Nanoscale Adv.*, 2020, **2**, 4024

Surface *vs.* core N/S/Se-heteroatom doping of carbon nanodots produces divergent yet consistent optical responses to reactive oxygen species†

Xu Geng,[ab] Thomas R. Congdon, [a] Palapuravan Anees,[a] Andrea A. Greschner,[a] Fiorenzo Vetrone [a] and Marc A. Gauthier *[a]

Carbon nanodots (CNDs) have attracted substantial scientific curiosity because of their intriguing stimuli-responsive optical properties. However, one obstacle to the more widespread use of CNDs as transducers for *e.g.*, biodetection systems is incomplete knowledge regarding the underlying chemical changes responsible for this responsiveness, and how these chemical features can be engineered *via* the precursors chosen for CND synthesis. This study demonstrates that the precursor's functional groups play a key role in directing N/S/Se heteroatom dopants either towards the surface of the CNDs, towards the aromatic core, or towards small organic fluorophores in the core. Divergent optical properties, which were consistent amongst groups of CNDs prepared with similar precursors, were obtained including either a decrease or increase of fluorescence intensity in the presence of hydrogen peroxide. Moreover, CNDs were identified with orthogonal responsiveness to radical (hydroxyl radicals, $^{\bullet}OH$; down to 2.5 μM) *vs.* non-radical oxidants (H_2O_2; down to 50 μM), which suggests that control of the chemistry of CNDs *via* the choice of precursor could yield probes that are specific to certain sub-species of reactive oxygen species or entirely different molecules altogether, based on the way they chemically-modify the surface (respond faster) and core functional groups (respond slower) associated with chromophores/fluorophores of which the CNDs are composed.

Received 28th May 2020
Accepted 15th July 2020

DOI: 10.1039/d0na00439a

rsc.li/nanoscale-advances

1. Introduction

Carbon nanodots (CNDs) are an emerging class of metal-free and carbon-rich nanomaterial with intriguing properties. They have attracted substantial scientific curiosity because they can possess high fluorescence quantum yield, high photo-stability, excitation-dependent fluorescence, adjustable surface chemistry, and especially stimuli-responsive optical properties.[1–5] Indeed, this last feature has drawn considerable attention because of its usefulness as an optical transducer for the presence of various chemicals.[6–13] Concurrently, much exciting work is ongoing to understand how to control the optical properties of CNDs *via* their chemistry.[14] However, one of the major obstacles to the more widespread use of CNDs is the incomplete knowledge regarding their chemical structure and how the latter relates to the aforementioned properties. At present, high quantum yield is believed to be related to the presence of small organic fluorophores produced by the condensation of certain types of precursor molecules, such as L-cysteine with citric acid.[14] High photo-stability, moderate quantum yield, and excitation-dependent fluorescence are associated with fluorescent states of aromatic or graphenic (sub)nano-domains.[15] Moreover, pendant functional groups not only determine the surface chemistry of the CNDs, which influence their colloidal properties, but also influence the energy levels of the aromatic/graphenic domains.

Within this context, heteroatom doping has been explored as a means to control and tune the features above. However, while it is very likely that the surface *vs.* core features of CNDs play a pivotal role in optical responses towards analytes, little information is available on this topic. To contribute towards a better understanding of CNDs, this study explores the chemical and optical features of a series of five related CNDs produced by hydrothermal synthesis from citric acid and amino acids. The incorporation of heteroatoms *via* precursors containing different functional groups (thiol/selenol, disulfide/diselenide, thioether/selenoether) is used to promote N/S/Se heteroatom doping to core (*i.e.*, incorporated in the aromatic domains) *versus* surface locations (pendant solvent exposed functional groups). Sulfur and selenium heteroatoms are of interest because of their susceptibility to oxidation/reduction, which can make them responsive to biologically relevant concentrations of reactive-oxygen species (ROS).[13,16,17] The latter are associated with varied physiological processes and diseases (cancer, inflammation,

[a]*Institut National de la Recherche Scientifique (INRS), EMT Research Center, 1650 Boul. Lionel-Boulet, Varennes, J3X 1S2, Canada. E-mail: gauthier@emt.inrs.ca*
[b]*School of Basic Medical Science, Henan University, Kaifeng 475004, P. R. China*

† Electronic supplementary information (ESI) available. See DOI: 10.1039/d0na00439a

neurodegenerative diseases, *etc.*).[11,18,19] Results show that precursor functional groups do indeed play a key role on directing heteroatom dopants either towards the surface of the CNDs, towards their aromatic core, or towards the formation of small organic fluorophores. This, in turn had an important and predictable impact on surface chemistry, optical properties, and changes to these two parameters in the presence of oxidants. Remarkably, selective S/Se-doping of the core yielded CNDs that slowly lost fluorescence upon oxidation with ROS. In contrast, a rapid gain of fluorescence was observed for surface S/Se-doped CNDs. Moreover, the CNDs displayed a quantitative yet selective response to radical *vs.* non-radical oxidants, based on how their functional groups react with oxidants.

2. Results

2.1 Morphology, composition, and optical properties

The production of CNDs by hydrothermal synthesis from citric acid and amino acids takes place *via* a dehydration–polymerization mechanism.[6,7] Six CNDs were produced by this method using a series of structurally related double-nucleophile precursors containing N/S or N/Se heteroatoms: L-cysteine (C), L-selenocysteine (Se-C), L-cystine (C_2), L-selenocystine (Se-C_2), L-methionine (M), and L-selenomethionine (Se-M). The morphologies of five out of the six heteroatom doped CNDs were characterized by transmission electron microscopy (Fig. 1a). All CNDs had a quasi-spherical shape with average diameters in the range of 1.5–2.5 nm. The absence of electron diffraction patterns in these images, as well as our inability to obtain quality Raman spectra for these entities (data not shown) suggests that the CNDs are essentially amorphous (*i.e.*, no pristine graphenic nanodomains). Our failure to image CNDs produced with Se-C by TEM, coupled to the absence of fluorescence for these CNDs suggested that selenol groups interfered with their hydrothermal synthesis. Indeed, selenols are substantially more nucleophilic than thiols and can also act as catalytic agents for the generation of ROS,[20] which could possibly contribute to degrading the structure of the CNDs. These CNDs were not further characterized. In other works, the incorporation of selenium heteroatoms into CNDs by hydrothermal synthesis was achieved using *e.g.*, sodium selenite,[21] Se-M,[22] or Se-C_2 precursors,[13] while sodium hydrogen selenide was used for doping pre-formed graphene oxide quantum dots.[12] Elemental analysis (Fig. 1b; full XPS survey spectra in Fig. S1†) revealed that all CNDs possess the expected heteroatoms. Highest N/S/Se doping was achieved using M and Se-M, and a range of quantum yields were observed for the CNDs

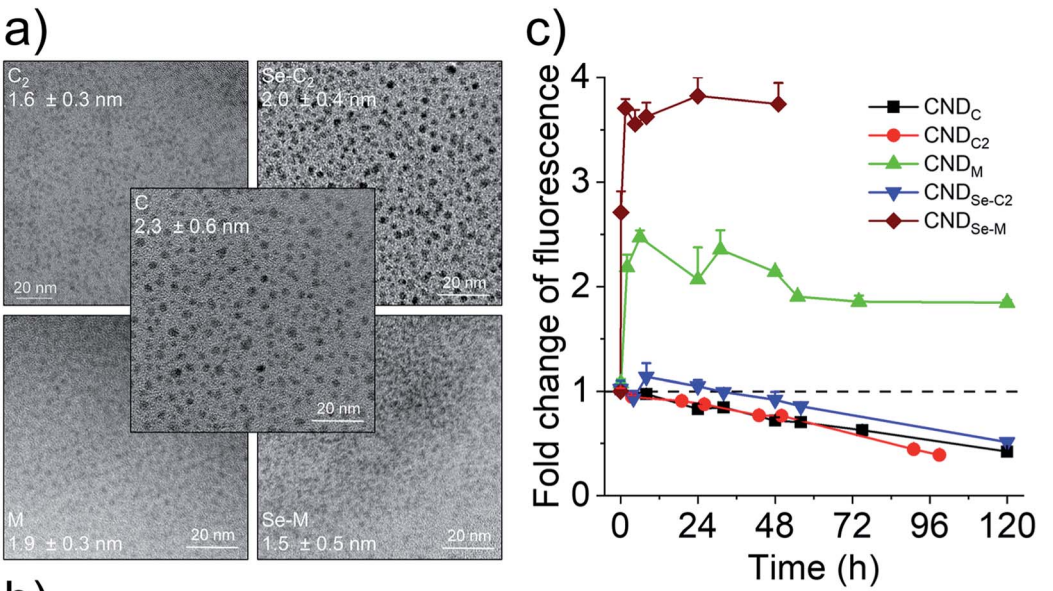

b)

Name	Precursor	C	O	N	S	Se	Quantum Yield
CND_C	Cysteine	77%	21%	1%	0.5%	–	90 ±10%
CND_{Se-C}	Selenocysteine	–	–	–	–	–	0%
CND_{C2}	Cystine	69%	27%	2%	1%	–	31 ±1%
CND_{Se-C2}	Selenocystine	72%	25%	2%	–	1%	3.9 ±0.3%
CND_M	Methionine	72%	19%	4%	5%	–	2.5 ± 0.1%
CND_{Se-M}	Selenomethionine	73%	20%	5%	–	2%	0.7 ±0.1%

Fig. 1 Structure, composition, and optical characteristics of CNDs. (a) Representative TEM images of CNDs and average particle size. (b) Elemental composition of CNDs by XPS, and fluorescence quantum yield. (c) Evolution of fluorescence emission of CNDs (λ_{ex} 360 nm; λ_{em} is the maximum emission wavelength seen in subsequent figures) in the presence of 50 mM H_2O_2. Data presented as mean + SD, $n = 3$.

(high for C and C2, low for the rest; Fig. 1b). Remarkably, both losses and gains of fluorescence were observed for different groups of structurally-related CNDs in the presence of hydrogen peroxide (H_2O_2; Fig. 1c). As seen in Fig. 1c, H_2O_2 can oxidize surface and core functional groups based on their accessibility and susceptibility to oxidation, which in turn influences fluorescence intensity. Note that the fluorescence intensities of all CNDs were stable for at least four days in the presence of very low concentrations of H_2O_2, demonstrating that these changes are specifically related to oxidation and not some form of instability (Fig. S2†). To rationalize this phenomenon, the location of heteroatom dopants as well as the influence of oxidation on the chemistry of the CNDs was investigated.

2.2 Core N,S and surface N-doped CNDs produced with C

Cysteine possesses two nucleophilic functional groups (thiol and amine), which are expected to readily react with citric acid to produce organic fluorophores in the early stages of the condensation–polymerization reaction (such as those proposed by Kasprzyk *et al.*),[14] in addition to aromatic domains due to the carbonization of citric acid. The high quantum yield observed for CND_C, similar to that reported by others (70–80%),[23,24] alongside the absence of excitation-dependent fluorescence corroborates this expectation (emission spectrum profile does not depend on excitation wavelength; Fig. 2a). Further analyzing these CNDs by ^{1}H NMR spectroscopy enabled the characterization of the most mobile and solvent-accessible functional groups on the CNDs, presumably those on their surface. Signals from rigid structures and solvent-inaccessible functional groups (within the core) are generally not observed using typical acquisition parameters. As suggested by Fig. 2b, the surface of CND_C bears residual carboxylic acid functional groups from the incomplete carbonization of citric acid. Moreover, the quartet at 3.7 ppm and doublet at 1.4 ppm, combined with the absence of

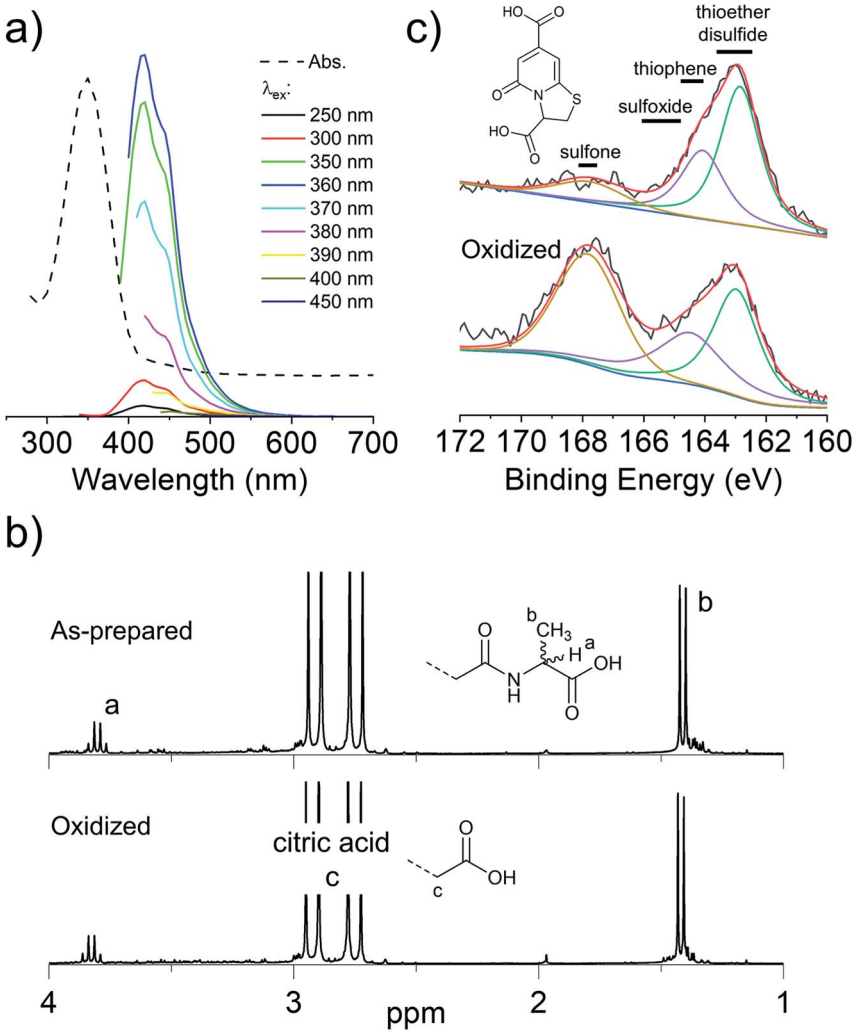

Fig. 2 CNDs produced from citric acid and cysteine are core S,N-doped, surface N-doped, and possess high quantum yield small organic fluorophores. (a) Absorbance and excitation-dependent fluorescence spectra; (b) ^{1}H NMR spectra before and after oxidation with H_2O_2 with possible pendant alanine-type structure shown in inset; (c) high-resolution XPS spectra for S_{2p} before and after oxidation with H_2O_2. Inset shows the structure of the putative fluorophore produced by condensation of citric acid and cysteine, as reported by Kasprzyk *et al.* (ref. 14). Spectral decomposition of the XPS is used to guide the eye and not to identify individual chemical species, owing to the diversity of such species expected within CNDs.

signals characteristic of the alkyl thiol from cysteine, suggests that cysteine on the surface of the CND is undergoing a thermal desulfurization reaction, leading to a structure resembling alanine. These observations are also reflected by ^{13}C NMR spectroscopy (Fig. S3†) with resonances at 17 ppm and 50 ppm that are similar to those of alanine. In light of the absence of S heteroatoms at the surface of CND_C, it is expected that the S heteroatoms are preferentially located in the core, while N heteroatoms are present at least partially on the surface in the form of alanine-type pendant functional groups. XPS analysis of the CNDs confirms the presence of thioether- and thiophenic groups, alongside amide-, pyridinic-, and pyrrolic-type nitrogen structures, which can be assigned to the core of the CNDs (Fig. 2c and S8†). Oxidation with H_2O_2 led to a very slow decrease of fluorescence over a period of several days (Fig. 1c). The appearance of sulfonic species was observed alongside an extensive decrease of thioether species, as well as partial oxidation of nitrogen groups (Fig. 2c and S8†). This suggests that degradation of the heterocyclic fluorophore is required to disrupt fluorescence. Moreover, the retention of the peaks from thiophenic S heteroatoms suggests that S heteroatoms in the core (*i.e.*, other than those associated with the small fluorophore) are not readily oxidized. Oxidation of amide nitrogen on the surface of CND_C did not occur under these conditions, based on ^1H and ^{13}C NMR data (Fig. 2b and S3†).

The use of C as precursor thus led to alanine-type surface functional groups (*i.e.*, "N-doped"), an S,N-doped aromatic core, and to high quantum yield small molecule fluorophores concealed in the core. Data suggests that degradation of the fluorophore is the dominant mechanism of loss of fluorescence intensity for CND_C in the presence of H_2O_2. The remaining N-heteroatoms on the surface and the S,N heteroatoms in the core changed little by oxidation under the conditions tested.

2.3 Core $N,S_{(ox)}/Se_{(ox)}$- and surface N-doped CNDs produced with C_2/Se-C_2

C_2 and Se-C_2 are oxidized forms of C and Se-C, respectively, which do not possess thiol or selenol nucleophiles. Both of these precursors possess two amino groups and therefore should behave as double nucleophiles in the CND fabrication reaction, at least in the initial stages of the hydrothermal reaction. Homolytic scission of the disulfide/diselenide bonds is not expected to occur at the temperatures used in the hydrothermal process.[25] Both precursors are insoluble in the citric acid in water mixture, requiring the addition of HCl to achieve solubility. In the literature, the acidic hydrolysis of C_2 and Se-C_2 in 6 M HCl at 110 °C has been reported to produce dehydroalanine, followed by pyruvate, ammonia, and small amounts of alanine.[26] Under the considerably less acidic conditions used herein, ^1H NMR spectroscopy revealed that the surface of CND_{C2} and $CND_{Se\text{-}C_2}$ is dominated by signature peaks for citric acid and alanine (as for CND_C), but no dehydroalanine (Fig. S4 and 5†). The elemental composition (Fig. 1b) of CND_{C_2} was similar to that of CND_C. Interestingly, S and Se heteroatoms in the as-synthesized $CND_{C_2/Se\text{-}C_2}$ already show signs of substantial oxidation (Fig. 3a and b), which contrasts to CND_C (Fig. 2c; where only thioether and thiophenic peaks were observed). Similar to CND_C, CDN_{C_2} did not exhibit excitation-dependent fluorescence (Fig. 3c). This could suggest the presence of a small organic fluorophore (possibly in a partially oxidized form, which would explain lower quantum yield than CND_C), which possesses the same two emissions as CND_C (*i.e.*, 425 and 450 nm), though the relative intensity of these two peaks was different. An alternative or additional interpretation is that the oxidation of S-heteroatoms in CND_{C_2} renders more uniform the functional groups associated with aromatic fluorophores, which can eliminate the excitation-dependence of fluorescence, albeit the quantum yield is too high for this explanation to be plausible.[15] This interpretation is in line with the XPS data (Fig. 3a and b) whereby only a small increase of sulfoxide/sulfone peak intensity was observed following oxidation with H_2O_2. However, as argument in favor of the formation of small organic fluorophores in CND_{C_2}, the emission spectrum of $CND_{Se\text{-}C_2}$ showed clear excitation-dependence (Fig. 3d). This, in combination with low quantum yield of $CND_{Se\text{-}C_2}$ (<10%) suggests emission from core aromatic domains. Exposure of both CNDs to H_2O_2 yielded a slow loss of fluorescence signal over 72 h (Fig. 1c) as well as a significant change in the N_{1s} signals as observed by XPS (Fig. 3a and b).

The use of C_2 and Se-C_2 precursors leads to alanine-type surface functional groups (N-doped) and $N,S_{(ox)}/Se_{(ox)}$-doped core aromatic domains. The combined data suggests that the dominant mechanism of loss of fluorescence quantum yield for CND_{C_2} and $CND_{Se\text{-}C_2}$ by H_2O_2 is oxidation of core N-heteroatoms. The remaining N-heteroatoms on the surface of $CND_{C_2/Se\text{-}C_2}$ as well as the S/Se-heteroatoms in the core of the CNDs (already oxidized during synthesis) were insensitive to further oxidation by ROS under the conditions tested.

2.4 Core and surface N,S/Se-doped CNDs produced with M/Se-M

To overcome the loss of surface S/Se heteroatoms due to precursor decomposition during hydrothermal synthesis, the latter were incorporated into the CNDs *via* thioether and selenoether precursors. Thioethers and selenoethers are weak nucleophiles that can be alkylated under certain conditions.[27] However, in the present context, reaction with carboxylic groups on citric acid is not expected as the resulting structures would be highly unstable. The CNDs produced with these two precursors both possessed quantum yields <10% and displayed important excitation-dependent fluorescence (Fig. 4a and b). This suggests that fluorescence results from a population of aromatic core fluorophores. Compared to the CNDs above, the level of incorporation of N,S/Se heteroatoms was substantially greater (Fig. 1b) despite the fact that M and Se-M behave more as single nucleophiles than as double nucleophiles. This could indicate that thio/selenoethers are more stable to the conditions encountered during hydrothermal synthesis. Indeed, ^1H and ^{13}C NMR spectroscopy shows that the thio/selenoether functional groups remain intact on the surface of CNDs, which is in contrast to the CNDs above for which the S/Se heteroatoms on the surface were always lost

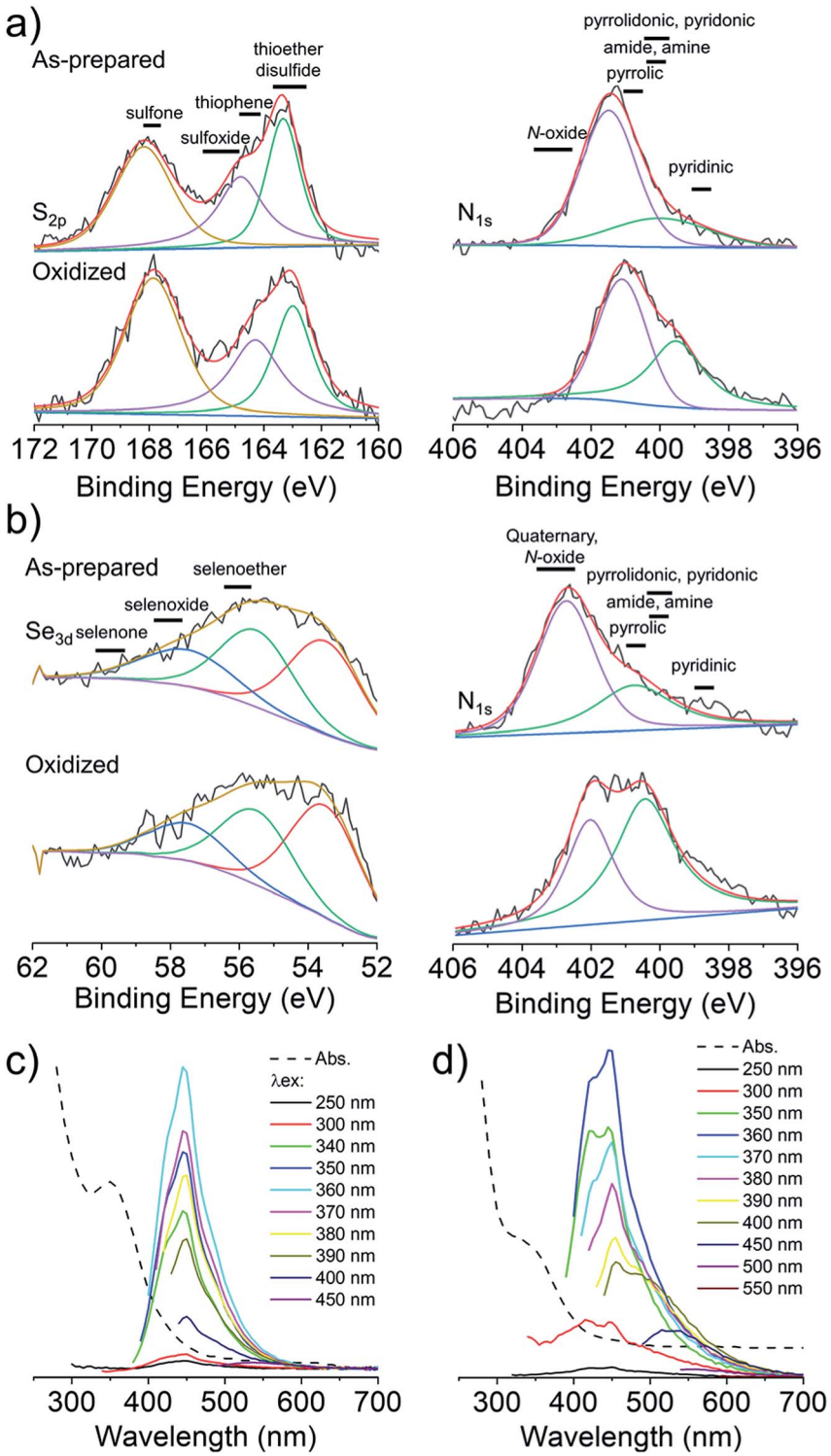

Fig. 3 CNDs produced from citric acid and C_2/Se-C_2 are surface N-doped and core N,$S_{(ox)}$/$Se_{(ox)}$-doped. High-resolution XPS spectra (S_{2p}, N_{1s}) before and after oxidation with H_2O_2 of CND_{C_2} (a) and $CND_{Se\text{-}C_2}$ (b). Spectral decomposition of the XPS spectra was performed to guide the eye. Absorbance and excitation-dependent fluorescence spectra of CND_{C_2} (c) and $CND_{Se\text{-}C_2}$ (d).

(Fig. 5a, b, S6 and S7†). Interestingly, oxidation led to a rapid 200–400% increase of fluorescence emission (<1 h; Fig. 1c), which contrasts with the very slow (days) decrease of fluorescence observed for all other CNDs above. As established by ^{1}H NMR spectroscopy (Fig. 5a), oxidation of CND_M leads to a quantitative conversion of surface thioether peaks to those of a sulfoxide. This is also observed by XPS (Fig. 4c). The absence of other significant changes to C_{1s} and N_{1s} signals (Fig. S11†) suggests that oxidation of surface thioether groups is responsible for the rapid increase of fluorescence intensity.

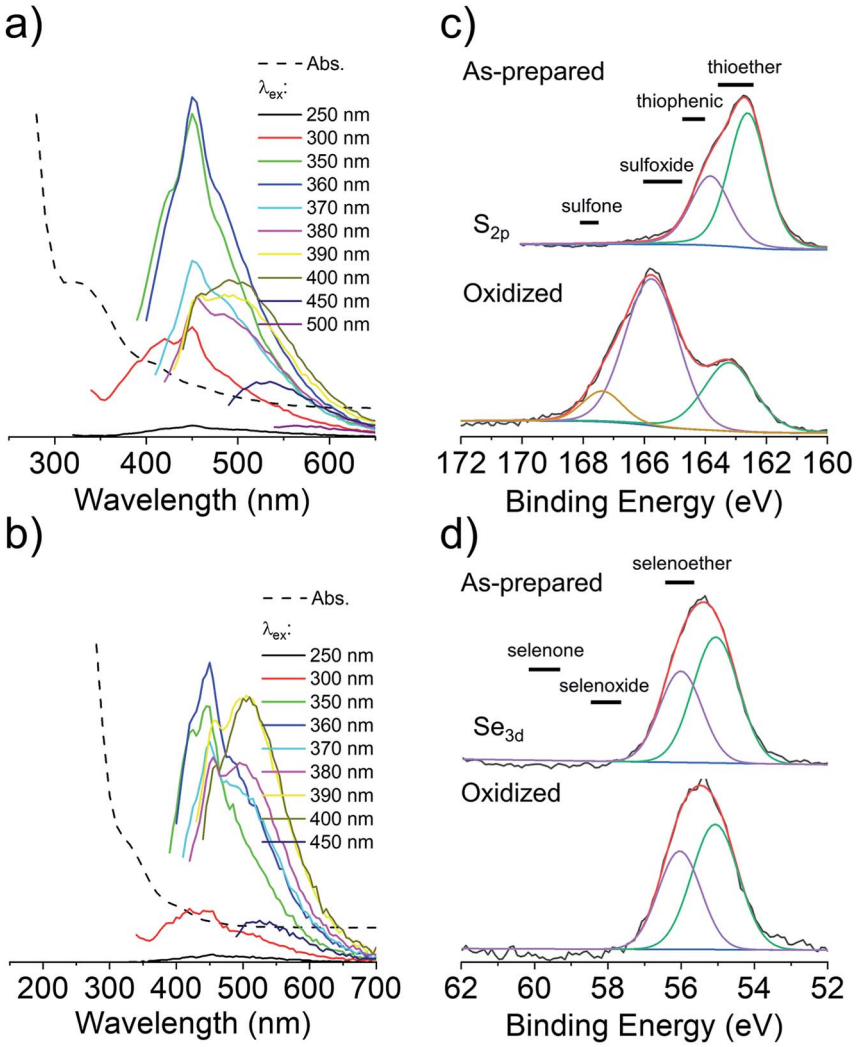

Fig. 4 CNDs produced from citric acid and M/Se-M are surface and core N,S/Se-doped. Absorbance and excitation-dependent fluorescence spectra of CND_M (a) and $CND_{Se\text{-}M}$ (b). High-resolution XPS spectra (S_{2p}, Se_{3d}) before and after oxidation with H_2O_2 of CND_M (c) and $CND_{Se\text{-}M}$ (d). Spectral decomposition of the XPS spectra was performed to guide the eye.

The presence of residual thioether/thiophenic sulfur after oxidation was observed by XPS (Fig. 4c), suggesting that certain S-doped functional groups in the core are less responsive to oxidation. Indeed, following the initial (rapid) increase of fluorescence caused by oxidation of surface thioether groups, a decrease of fluorescence was observed over a much longer period, synonymous with oxidation of core heteroatoms as seen above for the other CNDs. The results obtained with Se-M were similar to those for M, in that intact selenoether groups are observed on the surface of the CNDs by ^{1}H NMR spectroscopy (Fig. 5b) and that oxidation of these led to a rapid increase of fluorescence. In contrast, however, the ^{1}H NMR spectrum of the oxidized $CND_{Se\text{-}M}$ was not sufficiently clear to identify the structure of the oxidized surface functional groups. Indeed, selenoxides can undergo both elimination reactions and cyclization to selenuranes,[28] which could be responsible for the observed changes to the spectrum after oxidation. However, as the XPS Se_{3d} signal from $CND_{Se\text{-}M}$ (Fig. 4d) did not change significantly after oxidation, it is most likely that selenoxide elimination is occurring, which would leave behind only core Se-heteroatoms. The latter were insensitive to oxidation under the conditions examined, and consequently no decrease of fluorescence signal with prolonged oxidation, as seen for CND_M, was observed in Fig. 1c. Indeed very little or no change in the N_{1s} signal was observed upon oxidation of either CND_M or $CND_{Se\text{-}M}$ (Fig. S11 and 12†), which suggests that only S/Se heteroatoms are involved in the fluorescence increase (and subsequent decrease for CND_M).

Overall, the use of M/Se-M as precursor leads to pendant thioether/selenoether surface functional groups and N,S/Se-doped core aromatic domains. The collective data suggests that oxidation of the surface S/Se-heteroatoms leads to a rapid (<1 h) increase of fluorescence, but also to the concurrent elimination of surface Se heteroatoms. Slow oxidation of core S-heteroatoms caused a subsequent decrease of fluorescence for CND_M, while the oxidation of core Se heteroatoms did not occur for $CND_{Se\text{-}M}$ under the conditions examined.

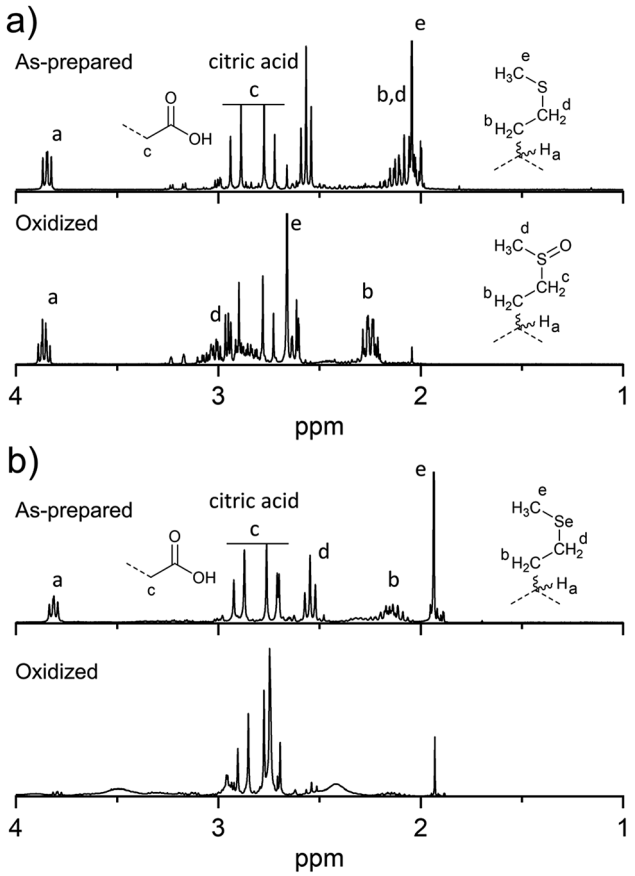

Fig. 5 Changes to surface chemistry of $CND_{M/Se-M}$ in response to H_2O_2. ^1H NMR spectra of CND_M (a) and CND_{Se-M} (b) before and after oxidation with H_2O_2.

2.5 Quantitative response to radical *vs.* non-radical ROS

In light of our ability to control the location of heteroatom doping for the CNDs, as well as our understanding of the chemical transformation that occurs in the presence of H_2O_2, an exploration of the quantitative relationship between fluorescence and the presence of ROS was undertaken. It is currently thought that the nature of the (heteroatom-containing) functional groups connected to or within the carbon framework of CNDs influence the energy levels of surface/core aromatic chromophores and fluorophores. This can lead, for instance, to excitation-dependent fluorescence when multiple different fluorescent species are present within a given CND. As such, the chemical changes to CNDs described above can lead to a change in the number and type of chromophores/fluorophores, resulting in *e.g.*, an increase or decrease of fluorescence. While the underlying structure–property relationships remain difficult to elucidate, in the present case the oxidation of the CNDs led to very minor changes to their absorption spectrum, with the exception of CND_{C2} for which a new peak below ~300 nm appeared (Fig. S13†). At 360 nm, the wavelength chosen to induce fluorescence in Fig. 6, increases/decreases of absorbance were consistent, yet not proportional, to the observed increase/decrease of fluorescence. This suggests the existence of a substantial population of non-fluorescent species that absorb at 360 nm and is consistent with the generally low quantum yield values (Fig. 1b). No additional peaks or shifts in the fluorescence spectrum were observed upon oxidation to explain changes of fluorescence intensity. Fig. 6a shows the changes of fluorescence of the CNDs in the presence of different concentrations of H_2O_2 spanning 4-orders of magnitude. The curves are plotted for a certain fixed reaction time, which was different for each CND owing to their different response kinetics to oxidation. The full time course evolution of fluorescence at each concentration of H_2O_2 for each CND is provided in Fig. S2.† It was interesting to note that linear responses (R^2 0.96–0.99) to H_2O_2 concentration were observed for all CND samples over 2–4 orders of magnitude of concentration in the 50 μM to 50 mM range, which encompasses the range of biological relevance

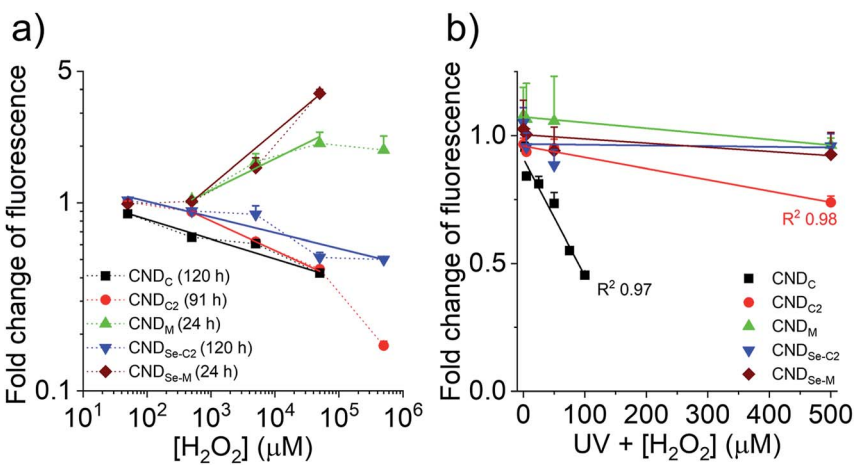

Fig. 6 Oxidation dependent fluorescence of CNDs. (a) Concentration-dependent change of fluorescence emission of CNDs in the presence of H_2O_2 (log–log scale) for a duration indicated between parentheses in the legend (λ_{ex} 360 nm; λ_{em} is the maximum emission wavelength seen in preceding figures). R^2 was 0.96–0.99 for all linear fits. (b) Concentration-dependent change of fluorescence emission of CNDs (linear scale) after 30 min exposure to H_2O_2 and UV radiation to produce hydroxyl radicals. For both panes, data presented as mean + SD, $n = 3$.

(50–100 μM).[29] Fluorescence intensity decreased for $CND_{C,C_2,Se\text{-}C_2}$ and increased for $CND_{M,Se\text{-}M}$ as expected from Fig. 1c. Deviations from linearity were sometimes observed at low H_2O_2 concentration and at high concentration, where the effect seemed to either to saturate (CND_M) or be enhanced (CND_{C_2}; the latter possibly indicating that more than one mechanism of inactivation is at play).

Considering that the response of the CNDs towards H_2O_2 was very slow for $CND_{C,C_2,Se\text{-}C_2}$ (days), it was considered warranted to explore whether a more rapid response to oxidation could be achieved with more reactive ROS.[30] As such, the change in optical properties of the CNDs was examined under ultraviolet (UV) irradiation in the presence of H_2O_2, to generate hydroxyl radicals (•OH) *in situ*.[31] Moreover, optical properties were measured after a period of 30 min of UV irradiation. In contrast to the non-radial oxidant H_2O_2, hydroxyl radicals are substantially more reactive and, as seen in Fig. 6b, much lower concentrations of H_2O_2 were employed in this series of experiments. Under these conditions, CND_C and CND_{C_2} showed a strong linear dependence on fluorescence emission with oxidant concentration over the 2.5–500 μM range ($R^2 > 0.97$). CND_C was more sensitive to this oxidant than CND_{C_2} and UV light alone did not influence its fluorescent properties (Fig. S14†). Intriguingly, under these same conditions, none of the other CNDs exhibited a change in their fluorescence output. This was especially surprising in the case of CND_M and $CND_{Se\text{-}M}$, which displayed a rapid and important response to H_2O_2 (Fig. 6a). This result can be reconciled by the fact that Hiller *et al.* have shown that the mechanism of oxidation of the thioether of methionine with hydroxyl radicals is substantially different from that with H_2O_2,[32] leading to a variety of possible structures, but not a sulfoxide. This observation highlights the importance of documenting chemical changes that occur to CNDs in response to a given stimulus, as the resulting chemical changes may produce very different optical effects. Indeed, the orthogonal responsiveness of CND_C and CND_M to the radical oxidant (•OH) and to the non-radical oxidant H_2O_2 is one example of how contradictory observations could be reported in the literature if the underlying chemical changes, even for related 'oxidizing' reactions, are not fully considered.

3. Conclusion

This study demonstrates that the precursor's functional groups play a key role in directing N,S/Se heteroatom dopants either towards the surface of the CNDs, towards the aromatic core, or towards small organic fluorophores in the core. C, C_2, and Se–C_2 partially decomposed during the hydrothermal process yielding core N,S/Se-doped CNDs whose fluorescence intensity decreased slowly by exposure to H_2O_2. In contrast, M and Se-M yielded both core and surface N,S/Se-doped CNDs whose fluorescence increased rapidly due to surface oxidation by H_2O_2. The CNDs therefore possessed divergent optical properties that correlated to changes to functional groups caused by exposure to ROS. Moreover, CNDs were identified with orthogonal responsiveness to radical *vs.* non-radical oxidants, a phenomenon that highlights the importance of documenting the specific chemical changes that occur upon exposure to a given reagent. This information could provide guidelines for preparing probes that are specific to certain sub-species of ROS or entirely different molecules altogether, based on basic organic chemistry reactions involving functional groups in different parts of the CND.

4. Experimental

4.1. Materials

Borohydride (polymer-supported, 20–50 mesh, extent of labeling: ~2.5 mmol g^{-1} loading), citric acid, L-cysteine (C), L-cystine (C_2), L-methionine (M), hydrochloric acid (37%), hydrogen peroxide (30% W/W in H_2O), quinine sulfate, and sodium hydroxide were purchased from Sigma-Aldrich. L-Selenocystine (Se-C_2), and L-selenomethionine (Se-M) were purchased from Fisher Scientific. Dialysis membranes (MWCO 500–1000) were purchased from Spectrum Labs (Ottawa, Canada). A non-stirred poly(tetrafluoroethylene)-lined (PTFE) pressure vessel (Model 4744, 45 mL) was purchased from Parr Instrument Company (Moline, IL). Ultrapure water was from a Milli-Q system (18.2 MΩ).

4.2. Synthesis of heteroatom-doped CNDs

CNDs were prepared by one-step hydrothermal synthesis. The precursor solutions for the heteroatom-doped carbon dots were prepared using similar protocols, with only slight variations in the composition. In all cases, the molar ratio between citric acid and amino acid remained constant. Cysteine: citric acid (0.75 g; 3.57×10^{-3} mol) and L-cysteine (0.3 g, 2.48×10^{-3} mol) were dissolved in water (8 mL). The solution was transferred to the pressure vessel and the solution bubbled with nitrogen for 30 min to remove dissolved oxygen.[33] Methionine: citric acid (0.75 g, 3.57×10^{-3} mol) and L-methionine (0.37 g, 2.48×10^{-3} mol) were dissolved in 8 mL water. Cystine: citric acid (0.375 g, 1.78×10^{-3} mol), L-cystine (0.149 g, 6.20×10^{-4} mol), and 1 M HCl (3 mL, 3×10^{-3} mol) were added to 8 mL water. Selenocystine: citric acid (0.375 g, 1.78×10^{-3} mol), L-selenocystine (0.207 g, 6.20×10^{-4} mol), and 1 M HCl (3 mL, 3×10^{-3} mol) were added to 8 mL water. Selenomethionine: citric acid (0.375 g, 1.78×10^{-3} mol) and L-selenomethionine (0.243 g, 1.24×10^{-3} mol) were added to 8 mL water. Selenocysteine: L-selenocystine (0.207 g, 6.20×10^{-4} mol) dissolved in 0.5 M NaOH (5 mL, 2.5×10^{-3} mol) and added to 2 g of polymer-supported borohydride (8 molar eq. relative to L-selenocystine) and 10 mL of water, while stirring, to reduce the diselenide bond. The flask was chilled to slow the release of hydrogen. Once the solution turned from yellow to colorless, it was aspirated with a syringe tipped with a 0.22 μm filter (leaving behind the polymer-supported reducing agent) and mixed with citric acid (0.375 g, 1.78×10^{-3} mol), then transferred to the pressure vessel.

Once the precursor solutions above were loaded into the pressure vessel, the latter was sealed and heated to 160 °C in an air oven (Quincy Lab, Inc. model 10 lab oven) for 5 h in a chemical fume hood. After this period, the vessel was cooled to room temperature and the contents dialysed (MWCO 500–1000) against 1 L of water for 3 days, with thrice-daily water

changes. The contents of the dialysis bag were recovered as a white or light yellow solid by lyophilisation and stored. The amount of recovered solid ranged from 8–152 mg for the six CNDs.

4.3. Characterization

The UV-visible absorption and fluorescence emission spectra of the CNDs were measured with a Cytation 5 microplate reader (Biotek, Vermont). Water was used as a blank for background subtraction. Excitation and emission wavelengths are mentioned where appropriate in the Results section. For transmission electron microscopy (TEM), a drop of CND solution in water was deposited onto a formvar/carbon coated copper grid (FCF300–Cu, Electron Microscopy Sciences) and left to dry at room temperature. Images were recorded with a JEM-2100F microscope (Japan) operating at 200 kV. ^{1}H and ^{13}C nuclear magnetic resonance spectroscopy was performed using a Bruker Ultrashield spectrometer operating at 300 MHz for protons, using D_2O as a solvent. X-ray photoelectron spectroscopy (XPS) was performed using a VG ESCALAB 220i-XL spectrometer equipped with a hemispherical analyzer for a Twin Al Anode X-ray Source. The instrument resolution was 0.75 eV. The C_{1s} peak (284.6 eV) was used as the reference line to accurately determine the positions of other spectral lines.

4.4. Measurement of fluorescence quantum yield (QY)

The quantum yield of the CNDs was determined using a reference point method.[23,34] Quinine sulfate in 0.1 M H_2SO_4 (literature quantum yield: 54%) was used as a standard to calculate the quantum yield of the CNDs dispersed in ultrapure water. The emission spectrum of the solutions at 360 nm excitation was measured. In order to minimize re-absorption effects, absorbance intensity was kept below 0.1.[35] Quantum yield was calculated using the formula below, where Φ represents quantum yield, Abs represents absorbance, A represents area under the fluorescence curve, and η the refractive index of the medium. The subscripts S and R denote the corresponding parameters for the sample and reference, respectively.

$$\frac{\Phi_S}{\Phi_R} = \frac{A_S}{A_R}\frac{(Abs)_R}{(Abs)_S}\frac{{\eta_S}^2}{{\eta_R}^2}$$

4.5. Response to hydrogen peroxide and hydroxyl radicals

Solutions of CND_C (1 μg mL^{-1}), CND_{C_2} (0.5 mg mL^{-1}), CND_M (6 mg mL^{-1}), $CND_{Se\text{-}C_2}$ (4.5 mg mL^{-1}), and $CND_{Se\text{-}M}$ (11 mg mL^{-1}) were prepared in 200 mM phosphate buffer pH 7.4 containing different concentrations of fresh H_2O_2. Fluorescence spectra (λ_{ex} = 360 nm; λ_{em} = 400–700) of these solutions were measured at predetermined intervals. For the detection of $^{\bullet}OH$, the solutions were exposed to UV light from a UVGL-15 UV lamp (256 nm, 4 W) for 30 min. Following UV irradiation, a fluorescence spectrum (λ_{ex} = 360 nm; λ_{em} = 400–700) was immediately recorded. To examine chemical changes to the CNDs after oxidation (samples exhibiting substantial changes to their fluorescence), hydrogen peroxide was removed by dialysis (MWCO of 500–1000) against distilled water over 3 days (water changed three times daily), and CNDs recovered by lyophilization.

Author contributions

XG, FV, and MAG designed and conceived the study. XG performed all experiments, with the help of TRC, PA, and AAG. XG and MAG wrote the manuscript. All authors discussed the results and their implications, and commented on the manuscript at all stages.

Conflicts of interest

There are no conflicts to declare.

Acknowledgements

XG acknowledges a postdoctoral scholarship from the China Scholarship Council. TRC and PA acknowledge a postdoctoral scholarship from the Fonds de Recherche du Québec – Santé (FRQS). This work was further supported by the Natural Science and Engineering Council of Canada (RGPIN-2015-04254). MAG is a Research Scholar of the FRQS. AAG acknowledges postdoctoral scholarships from the Fonds de Recherche du Québec – Nature et Technologies and the Canadian Institutes for Health Research. Further, she acknowledges the Chu Family Scholarship for a career award. G Zhang, Q Wei, and S Sun are thanked for assistance with XPS. FV acknowledges funding from the Natural Sciences and Engineering Research Council (NSERC) of Canada through the Discovery Grants program and the Discovery Accelerator Supplement award, the Canada Foundation for Innovation for infrastructure and its operation, and the Fonds de Recherche du Québec – Nature et technologies (FRQNT).

Reference

1 H. Li, Z. Kang, Y. Liu and S.-T. Lee, Carbon nanodots: synthesis, properties and applications, *J. Mater. Chem.*, 2012, **22**(46), 24230–24253.
2 S. Y. Lim, W. Shen and Z. Gao, Carbon quantum dots and their applications, *Chem. Soc. Rev.*, 2015, **44**(1), 362–381.
3 P. Zuo, X. Lu, Z. Sun, Y. Guo and H. He, A review on syntheses, properties, characterization and bioanalytical applications of fluorescent carbon dots, *Microchim. Acta*, 2016, **183**(2), 519–542.
4 J. Zhou, H. Zhou, J. Tang, S. Deng, F. Yan, W. Li and M. Qu, Carbon dots doped with heteroatoms for fluorescent bioimaging: a review, *Microchim. Acta*, 2017, **184**(2), 343–368.
5 J. Wang and J. Qiu, A review of carbon dots in biological applications, *J. Mater. Sci.*, 2016, **51**(10), 4728–4738.
6 Y. Gong, B. Yu, W. Yang and X. Zhang, Phosphorus, and nitrogen co-doped carbon dots as a fluorescent probe for real-time measurement of reactive oxygen and nitrogen species inside macrophages, *Biosens. Bioelectron.*, 2016, **79**, 822–828.

7 W. Li, Z. Zhang, B. Kong, S. Feng, J. Wang, L. Wang, J. Yang, F. Zhang, P. Wu and D. Zhao, Simple and Green Synthesis of Nitrogen-Doped Photoluminescent Carbonaceous Nanospheres for Bioimaging, *Angew. Chem., Int. Ed.*, 2013, **52**(31), 8151–8155.
8 X. Shan, L. Chai, J. Ma, Z. Qian, J. Chen and H. Feng, B-doped carbon quantum dots as a sensitive fluorescence probe for hydrogen peroxide and glucose detection, *Analyst*, 2014, **139**(10), 2322–2325.
9 X. Jia, Y. Han, M. Pei, X. Zhao, K. Tian, T. Zhou and P. Liu, Multi-functionalized hyaluronic acid nanogels crosslinked with carbon dots as dual receptor-mediated targeting tumor theranostics, *Carbohydr. Polym.*, 2016, **152**, 391–397.
10 J. Chen, J. Liu, J. Li, L. Xu and Y. Qiao, One-pot synthesis of nitrogen and sulfur co-doped carbon dots and its application for sensor and multicolor cellular imaging, *J. Colloid Interface Sci.*, 2017, **485**, 167–174.
11 S. Bhattacharya, R. Sarkar, S. Nandi, A. Porgador and R. Jelinek, Detection of Reactive Oxygen Species by a Carbon-Dot–Ascorbic Acid Hydrogel, *Anal. Chem.*, 2017, **89**(1), 830–836.
12 S. Yang, J. Sun, P. He, X. Deng, Z. Wang, C. Hu, G. Ding and X. Xie, Selenium Doped Graphene Quantum Dots as an Ultrasensitive Redox Fluorescent Switch, *Chem. Mater.*, 2015, **27**(6), 2004–2011.
13 F. Li, T. Li, C. Sun, J. Xia, Y. Jiao and H. Xu, Selenium-Doped Carbon Quantum Dots for Free-Radical Scavenging, *Angew. Chem., Int. Ed.*, 2017, **56**(33), 9910–9914.
14 W. Kasprzyk, S. Bednarz and D. Bogdał, Luminescence phenomena of biodegradable photoluminescent poly(diol citrates), *Chem. Commun.*, 2013, **49**(57), 6445–6447.
15 J. Manioudakis, F. Victoria, C. A. Thompson, L. Brown, M. Movsum, R. Lucifero and R. Naccache, Effects of nitrogen-doping on the photophysical properties of carbon dots, *J. Mater. Chem. C*, 2019, **7**(4), 853–862.
16 K. Xu, M. Qiang, W. Gao, R. Su, N. Li, Y. Gao, Y. Xie, F. Kong and B. Tang, A near-infrared reversible fluorescent probe for real-time imaging of redox status changes in vivo, *Chem. Sci.*, 2013, **4**(3), 1079–1086.
17 J. T. Rotruck, A. L. Pope, H. E. Ganther, A. B. Swanson, D. G. Hafeman and W. G. Hoekstra, Selenium: Biochemical Role as a Component of Glutathione Peroxidase, *Science*, 1973, **179**(4073), 588–590.
18 N. K. Ojha, E. Leipold, R. Schönherr, T. Hoshi and S. H. Heinemann, Non-photonic sensing of membrane-delimited reactive species with a Na+ channel protein containing selenocysteine, *Sci. Rep.*, 2017, **7**, 46003.
19 H. Bayr, Reactive oxygen species, *Crit. Care Med.*, 2005, **33**(12), S498–S501.
20 C. W. Nogueira, G. Zeni and J. B. T. Rocha, Organoselenium and Organotellurium Compounds: Toxicology and Pharmacology, *Chem. Rev.*, 2004, **104**(12), 6255–6286.
21 G. Huang, Y. Lin, L. Zhang, Z. Yan, Y. Wang and Y. Liu, Synthesis of Sulfur-Selenium Doped Carbon Quantum Dots for Biological Imaging and Scavenging Reactive Oxygen Species, *Sci. Rep.*, 2019, **9**(1), 19651.
22 L. S. Walekar, M. Zheng, L. Zheng and M. Long, Selenium and nitrogen co-doped carbon quantum dots as a fluorescent probe for perfluorooctanoic acid, *Microchim. Acta*, 2019, **186**(5), 278.
23 S. Zhu, Q. Meng, L. Wang, J. Zhang, Y. Song, H. Jin, K. Zhang, H. Sun, H. Wang and B. Yang, Highly photoluminescent carbon dots for multicolor patterning, sensors, and bioimaging, *Angew. Chem.*, 2013, **125**(14), 4045–4049.
24 Y. Dong, H. Pang, H. B. Yang, C. Guo, J. Shao, Y. Chi, C. M. Li and T. Yu, Carbon-Based Dots Co-doped with Nitrogen and Sulfur for High Quantum Yield and Excitation-Independent Emission, *Angew. Chem., Int. Ed.*, 2013, **52**(30), 7800–7804.
25 V. A. Yablokov, Y. A. Vasina, I. A. Zelyaev and S. V. Mitrofanova, Kinetics of thermal decomposition of sulfur-containing amino acids, *Russ. J. Gen. Chem.*, 2009, **79**(6), 1141.
26 R. E. Huber and R. S. Criddle, Comparison of the chemical properties of selenocysteine and selenocystine with their sulfur analogs, *Arch. Biochem. Biophys.*, 1967, **122**(1), 164–173.
27 T. J. Deming, Functional Modification of Thioether Groups in Peptides, Polypeptides, and Proteins, *Bioconjugate Chem.*, 2017, **28**(3), 691–700.
28 J. A. Ritchey, B. M. Davis, P. A. Pleban and C. A. Bayse, Experimental and theoretical evidence for cyclic selenurane formation during selenomethionine oxidation, *Org. Biomol. Chem.*, 2005, **3**(24), 4337–4342.
29 C. de Gracia Lux, S. Joshi-Barr, T. Nguyen, E. Mahmoud, E. Schopf, N. Fomina and A. Almutairi, Biocompatible Polymeric Nanoparticles Degrade and Release Cargo in Response to Biologically Relevant Levels of Hydrogen Peroxide, *J. Am. Chem. Soc.*, 2012, **134**(38), 15758–15764.
30 C. C. Winterbourn, Reconciling the chemistry and biology of reactive oxygen species, *Nat. Chem. Biol.*, 2008, **4**(5), 278–286.
31 H. Ghodbane and O. Hamdaoui, Decolorization of antraquinonic dye, C.I. Acid Blue 25, in aqueous solution by direct UV irradiation, UV/H_2O_2 and UV/Fe(II) processes, *Chem. Eng. J.*, 2010, **160**, 226–231.
32 K. O. Hiller, B. Masloch, M. Goebl and K. D. Asmus, Mechanism of the hydroxyl radical induced oxidation of methionine in aqueous solution, *J. Am. Chem. Soc.*, 1981, **103**(10), 2734–2743.
33 Z.-C. Yang, M. Wang, A. M. Yong, S. Y. Wong, X.-H. Zhang, H. Tan, A. Y. Chang, X. Li and J. Wang, Intrinsically fluorescent carbon dots with tunable emission derived from hydrothermal treatment of glucose in the presence of monopotassium phosphate, *Chem. Commun.*, 2011, **47**(42), 11615–11617.
34 S. Karthik, B. Saha, S. K. Ghosh and N. P. Singh, Photoresponsive quinoline tethered fluorescent carbon dots for regulated anticancer drug delivery, *Chem. Commun.*, 2013, **49**(89), 10471–10473.
35 Q. Wang, X. Huang, Y. Long, X. Wang, H. Zhang, R. Zhu, L. Liang, P. Teng and H. Zheng, Hollow luminescent carbon dots for drug delivery, *Carbon*, 2013, **59**, 192–199.